Introducing Titratable Water to All-Atom Molecular Dynamics at Constant pH

Wei Chen, Jason A. Wallace, Zhi Yue, and Jana K. Shen*
Department of Pharmaceutical Sciences, School of Pharmacy, University of Maryland, Baltimore, Maryland

ABSTRACT Recent development of titratable coions has paved the way for realizing all-atom molecular dynamics at constant pH. To further improve physical realism, here we describe a technique in which proton titration of the solute is directly coupled to the interconversion between water and hydroxide or hydronium. We test the new method in replica-exchange continuous constant pH molecular dynamics simulations of three proteins, HP36, BBL, and HEWL. The calculated pK_a values based on 10-ns sampling per replica have the average absolute and root-mean-square errors of 0.7 and 0.9 pH units, respectively. Introducing titratable water in molecular dynamics offers a means to model proton exchange between solute and solvent, thus opening a door to gaining new insights into the intricate details of biological phenomena involving proton translocation.

Received for publication 6 April 2013 and in final form 25 June 2013.

*Correspondence: jshen@rx.umaryland.edu

Solution pH is an important factor in biology. Although neutral pH in extracellular medium accounts for balanced electrostatics and proper folding of protein structures, pH gradients across cell membranes induce large conformational changes that are necessary for biological functions, such as ATP synthesis and efflux of small molecules out of the cell. To gain detailed insights into pH-dependent conformational phenomena, several constant pH molecular dynamics (pHMD) methods, based on either discrete or continuous titration coordinates, have been developed in the last decade (1–4). In the continuous pHMD (CpHMD) framework (2,4), a set of titration coordinates $\{\lambda_i\}$ are simultaneously propagated along with the conformational degrees of freedom. Although the original CpHMD method based on the generalized Born (GB) implicit-solvent models (2,4) offers quantitative prediction of pK_a values and pH dependence of folding and conformational dynamics of proteins (5), its accuracy and applicability to highly charged systems and those with dominantly hydrophobic regions are limited due to the approximate nature of the underlying implicit-solvent models.

Motivated by the above-mentioned need, three groups have made efforts to develop a CpHMD method using exclusively the explicit-solvent models (6–8). In our development, the titration of acidic and basic sites is coupled with that of coions to level the total charge of the system (8). To further improve physical realism, here we replace the coions by titratable water molecules, which not only absorb the excess charge but also enable direct modeling of solute-solvent proton exchange in classical molecular dynamics simulations.

To illustrate the utility of the new methodology, we applied it to the titration simulations of three proteins that were previously used to benchmark the GB-based CpHMD. Although this work does not explore specific interactions between titratable waters and proteins, the methodology can be further tested or improved to provide a rigorous way for modeling proton transfer in molecular dynamics, which is a computationally efficient alternative to the empirical valence-bond theory-based methodologies (9,10).

We define titration of water as:

1. Loss of a proton to give a negatively charged hydroxide,

$$H_2O \rightleftharpoons OH^- + H^+, \quad (1)$$

or

2. Gain of a proton to give a positively charged hydronium,

$$H_2O + H^+ \rightleftharpoons H_3O^+. \quad (2)$$

We now couple the titration of hydroxide (Eq. 1) with that of an acidic site of the solute in the CpHMD simulation,

$$HA + OH^- \overset{K_a}{\rightleftharpoons} A^- + H_2O. \quad (3)$$

The use of hydronium is avoided here to prevent a potential artifact due to prolonged attraction with A^-. Analogously, we couple the titration of hydronium (Eq. 2) with that of a basic site,

$$BH^+ + H_2O \overset{K_b}{\rightleftharpoons} H_3O^+ + B. \quad (4)$$

Thus, effectively, a proton is transferred between the solute and solvent. However, we should note that in CpHMD simulations, titratable protons are represented by covalently attached dummies (2,4). Through varying the atomic charges and van der Waals interactions, they are seen by other atoms in the protonated state but not in the

Editor: Nathan Baker.

http://dx.doi.org/10.1016/j.bpj.2013.06.036

unprotonated state (see Table S1 in the Supporting Material). Furthermore, the solution proton concentration is implicitly modeled through a free energy term (2,4).

In CpHMD, the reference potential of mean force (PMF) for titration is that of the model compound (blocked single amino acid in water) along λ (2,4). In the presence of cotitrating water molecules, it is necessary to add the PMF for the conversion of water to hydroxide or hydronium. One-nanosecond NPT simulations at ambient pressure and temperature were performed to calculate the average force, $\langle dU/d,\theta\rangle$ at given θ-values, which are related to λ by $\lambda = \sin^2\theta$ (see Fig. S1 in the Supporting Material). Thermodynamic integration was then applied to calculate the PMF. We found that the average force can be accurately fit when assuming the PMF is quadratic in λ (Fig. 1). The same applies to the PMFs for titration of models Asp, Glu, and His. After testing on the titration of model compounds (see Table S2), we performed 10-ns all-atom CpHMD simulations with the pH replica-exchange protocol for three proteins: HP36, BBL and HEWL (see the Supporting Material for details). Most of the calculated pK_a values were converged in 10 ns per replica (see Fig. S3). Results are summarized in Table 1 and Fig. S4. Based on the 10-ns data, the root-mean-square (RMS) and average absolute errors are 0.9 and 0.7 pH units, respectively, while the largest absolute error is 2.5 (Glu^{35} of HEWL). Linear regression of the calculation versus experiment gives R^2 of 0.8 and slope of 1.2.

Breaking the simulations in two halves, we noticed that the second 5-ns sampling gave better agreement with experiment. The RMS deviation is reduced from 1.2 to 0.9 pH units, while the average absolute deviation is reduced from 1.0 to 0.6 pH units. The linear regression against experimental data is also improved, with the slope decreasing from 1.4 to 1.1 although R_2 remains the same. Comparing these second-half results with the GB-based simulations, we find that the RMS and average absolute deviations are about the same as the GB-CpHMD results; however, the all-atom simulations show a small systematic overestimation (regression slope >1), whereas GB simulations show a systematic underestimation (regression slope <1).

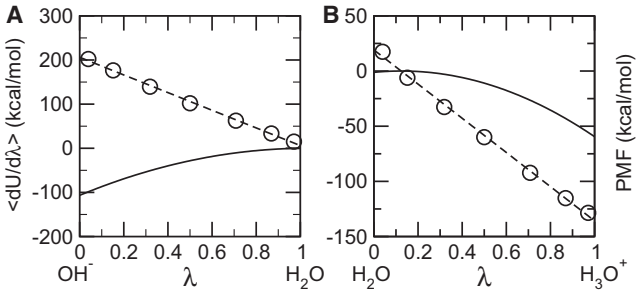

FIGURE 1 Average force and potential of mean force for converting a water molecule to hydroxide (*A*) and hydronium. (*B*) (*Data points*) Average forces. (*Dashed curves*) Best fits using a linear function, $2A(\lambda - B)$. (*Solid curves*) Corresponding potential of mean force.

TABLE 1 Calculated and experimental pK_a values of three proteins

	Experiment[a]	GB[a]	All-atom CpHMD		
Residue	Time (ns)[b]	0–1	0–5	5–10	0–10
HP36					
Asp^{44}	3.10 (0.01)	3.2 (0.1)	2.0	3.0	2.6 (0.5)
Glu^{45}	3.95 (0.01)	3.5 (0.1)	4.3	4.5	4.4 (0.1)
Asp^{46}	3.45 (0.12)	3.5 (0.1)	2.4	3.7	3.1 (0.6)
Glu^{72}	4.37 (0.03)	3.5 (0.1)	4.4	4.4	4.4 (0.0)
BBL					
Asp^{129}	3.88 (0.02)	3.2 (0.0)	2.2	3.2	2.7 (0.5)
Glu^{141}	4.46 (0.04)	4.3 (0.0)	4.0	4.4	4.2 (0.2)
His^{142}	6.47 (0.04)	7.1 (0.0)	5.9	5.8	5.8 (0.0)
Asp^{145}	3.65 (0.04)	2.8 (0.2)	3.0	3.1	3.1 (0.0)
Glu^{161}	3.72 (0.05)	3.6 (0.3)	4.2	3.9	4.0 (0.2)
Asp^{162}	3.18 (0.04)	3.4 (0.3)	2.9	3.5	3.2 (0.3)
Glu^{164}	4.50 (0.03)	4.5 (0.1)	5.7	4.6	5.2 (0.6)
His^{166}	5.39 (0.02)	5.4 (0.1)	4.4	4.4	4.4 (0.0)
HEWL					
Glu^{7}	2.6 (0.2)	2.6 (0.1)	3.6	3.4	3.5 (0.1)
His^{15}	5.5 (0.2)	5.3 (0.5)	5.1	5.1	5.1 (0.0)
Asp^{18}	2.8 (0.3)	2.9 (0.0)	2.5	3.3	2.9 (0.4)
Glu^{35}	6.1 (0.4)	4.4 (0.2)	8.5	8.7	8.6 (0.1)
Asp^{48}	1.4 (0.2)	2.8 (0.2)	−0.1	1.1	0.6 (0.6)
Asp^{52}	3.6 (0.3)	4.6 (0.0)	5.4	5.6	5.5 (0.1)
Asp^{66}	1.2 (0.2)	1.2 (0.4)	−0.6	0.8	0.3 (0.7)
Asp^{87}	2.2 (0.1)	2.0 (0.1)	0.8	2.1	1.5 (0.7)
Asp^{101}	4.5 (0.1)	3.3 (0.3)	6.1	5.7	5.9 (0.2)
Asp^{119}	3.5 (0.3)	2.5 (0.1)	3.0	3.3	3.2 (0.1)
Maximum absolute deviation		1.8	2.4	2.6	2.5
Average absolute deviation (RMS deviation)		0.5 (0.7)	1.0 (1.2)	0.6 (0.9)	0.7 (0.9)
Linear fit R^2 (slope)		0.7 (0.8)	0.8 (1.4)	0.7 (1.1)	0.8 (1.2)

[a]Taken from Wallace and Shen (12). The pK_a's of BBL were recalculated.
[b]Sampling time per pH replica.

The improvement in the second halves of the simulations are seen mainly for residues involved in attractive electrostatic interactions, including Asp^{44} and Asp^{46} of HP36, Asp^{129} of BBL, and Asp^{48}, Asp^{66}, and Asp^{87} of HEWL. These residues are initially locked in salt-bridges or hydrogen bonds. However, in the second 5 ns, the attractive interactions weakened, leading to a decrease in the calculated pK_a shifts relative to the model values and better agreement with experiment. For instance, Asp^{44} was initially in a salt-bridge distance from Arg^{55}. However, the salt-bridge positions were sampled less often in the second 5 ns (see Fig. S5), which explains the 1-unit reduction in the calculated pK_a shift. Significant fluctuation in ion-pair interactions was also observed in the work by Alexov (11). The carboxyl oxygen of Asp^{46} was a hydrogen-bond acceptor with both the backbone amide and hydroxyl of Ser^{43}. These hydrogen bonds were less frequently sampled in the second 5 ns (see Fig. S6), leading to a decrease of the pK_a shift for Asp^{46} by 1.3 units. These results indicate that extensive conformational sampling is necessary to give an accurate estimate of the ratio between the charged and neutral populations.

Limited conformational sampling is also a contributing factor to the overestimation of the pK_a shifts for buried residues (Table 1). In fact, we observed ionization-induced conformational changes for His^{166} of BBL and Glu^{35} of HEWL: they became more exposed to solvent when becoming charged as indicated by an increase in the solvent-accessible surface area (SASA) (see Fig. S7 and Fig. S8). The increase in SASA is correlated with the more frequent sampling of the states with λ close to 1, i.e., the deprotonated form (see Fig. S9). However, because Glu^{35} was buried in the starting conformation and the transition between buried and exposed states is slow compared to the simulation length, the exposed state may not be sufficiently sampled, leading to overestimation of the pK_a shift.

In contrast to Glu^{35}, the SASA of Asp^{52} in HEWL is almost identical for both protonation states. The lack of conformational fluctuation is due to the strong hydrogen bonding with the side-chain amino group of Asn^{46} and Asn^{59} (data not shown). Overestimation of the pK_a shifts for buried residues can also be attributed to the limitation of the additive force field which underestimates dielectric response in protein environment (more discussion see Supporting Material) of the pK_a shifts for buried residues.

Finally, to ascertain if the presence of hydroxide/hydronium introduces artifacts, we studied the interaction between hydroxide/hydronium and the titratable sites/ions. Comparing the hydroxide/hydronium with respective chloride/sodium ions, we find that the spatial distributions are nearly identical (see plots of distance distributions and radial distribution functions in Figs. S10–S13). However, the relative occupancy of the hydroxide around the neutral Asp/Glu, positive histidine, or sodium ion is 2–3 times as that of a chloride. The water-bridged interaction between sodium and chloride ions becomes much weaker when chloride is replaced by hydroxide or sodium is replaced by hydronium. By contrast, the occupancy of the hydronium around the solute is similar to that of the sodium. Furthermore, similar pK_a results for these proteins were obtained when coions were used instead of titratable waters (data not shown). Thus, we believe that potential artifacts related to the ionized forms of water are negligible. Work is underway to further understand the limitations of the methodology and to explore applications to protein dynamics coupled to proton transfer.

In summary, we have developed and tested titratable water models for use in all-atom CpHMD simulations. Although the benchmark pK_a calculations indicate a comparable accuracy as the GB-CpHMD method, the all-atom method offers physical rigor and most importantly, it is applicable to systems that cannot be studied with GB-based simulations such as lipids and nucleic acids. We anticipate that the accuracy of this methodology can be further improved by incorporating the new-generation force fields that account for polarization. The coupling between proton titration of water and solute offers a computationally efficient way to model proton transfer in molecular mechanics simulations.

SUPPORTING MATERIAL

Simulation details, two tables, and thirteen figures are available at http://www.biophysj.org/biophysj/supplemental/S0006-3495(13)00745-5.

ACKNOWLEDGEMENTS

The authors acknowledge the University of Oklahoma Supercomputing Center for computing time and the National Institutes of Health (grant No. RO1-GM098818) for funding.

REFERENCES and FOOTNOTES

1. Baptista, A. M., V. H. Teixeira, and C. M. Soares. 2002. Constant-pH molecular dynamics using stochastic titration. *J. Chem. Phys.* 117:4184–4200.
2. Lee, M. S., F. R. Salsbury, Jr., and C. L. Brooks, 3rd. 2004. Constant-pH molecular dynamics using continuous titration coordinates. *Proteins.* 56:738–752.
3. Mongan, J., D. A. Case, and J. A. McCammon. 2004. Constant pH molecular dynamics in generalized Born implicit solvent. *J. Comput. Chem.* 25:2038–2048.
4. Khandogin, J., and C. L. Brooks, 3rd. 2005. Constant pH molecular dynamics with proton tautomerism. *Biophys. J.* 89:141–157.
5. Chen, J., C. L. Brooks, 3rd, and J. Khandogin. 2008. Recent advances in implicit solvent-based methods for biomolecular simulations. *Curr. Opin. Struct. Biol.* 18:140–148.
6. Donnini, S., F. Tegeler, …, H. Grubmüller. 2011. Constant pH molecular dynamics in explicit solvent with λ-dynamics. *J. Chem. Theory Comput.* 7:1962–1978.
7. Goh, G. B., J. L. Knight, and C. L. Brooks, 3rd. 2012. Constant pH molecular dynamics simulations of nucleic acids in explicit solvent. *J. Chem. Theory Comput.* 8:36–46.
8. Wallace, J. A., and J. K. Shen. 2012. Charge-leveling and proper treatment of long-range electrostatics in all-atom molecular dynamics at constant pH. *J. Chem. Phys.* 137:184105.
9. Braun-Sand, S., M. Strajbl, and A. Warshel. 2004. Studies of proton translocations in biological systems: simulating proton transport in carbonic anhydrase by EVB-based models. *Biophys. J.* 87:2221–2239.
10. Swanson, J. M. J., C. M. Maupin, …, G. A. Voth. 2007. Proton solvation and transport in aqueous and biomolecular systems: insights from computer simulations. *J. Phys. Chem. B.* 111:4300–4314.
11. Alexov, E. 2003. Role of the protein side-chain fluctuations on the strength of pair-wise electrostatic interactions: comparing experimental with computed pK_as. *Proteins.* 50:94–103.
12. Wallace, J. A., and J. K. Shen. 2011. Continuous constant pH molecular dynamics in explicit solvent with pH-based replica exchange. *J. Chem. Theory Comput.* 7:2617–2629.

SUPPLEMENTAL MATERIAL

Introducing titratable water to all-atom molecular dynamics at constant pH

Wei Chen, Jason A. Wallace, Zhi Yue and Jana K. Shen*
Department of Pharmaceutical Sciences, School of Pharmacy, University of Maryland, Baltimore, MD 21201
*Corresponding author. Phone: (410) 706-4187; Fax: (410) 706-5017; E-mail: jshen@rx.umaryland.edu.

Simulation Details

Structure preparation

Three proteins were studied in this work: the 36-residue subdomain of villin headpiece, HP36 (PDB code 1VII), 45-residue binding domain of 2-oxoglutarate dehydrogenase multi-enzyme complex, BBL (PDB code 1W4H), and 129-residue hen egg white lysozyme, HEWL (PDB code 2LZT). The HBUILD facility of CHARMM was used to add hydrogens to the proteins. The N-termini were left free while the C-termini were N-methylamidated. The proteins were solvated in a truncated octahedral water box. The distance between the protein and the edges of the water box was at least 10 Å. Titratable co-ions (hydroxide and hydronium) were added for all titration sites (Asp, Glu, and His) to level the total net charge (1): 4 OH^- for HP36; 2 H_3O^+ and 6 OH^- for BBL; and 1 H_3O^+ and 9 OH^- for HEWL. Na^+ and/or Cl^- ions were then added to neutralize the system and reach the experimental ionic strength: 150 mM for for HP36 (2), 200 mM for BBL (3, 4), and 50 mM for HEWL (5). The model compounds were single amino acids acetylated at the N-terminus (ACE) and N-methylamidated at C-terminus (CT3). The model compounds were solvated in a cubic water box. For the simulation of model Asp and Glu, one hydroxide (interconverting with water) and one Na^+ counter-ion were added to the system, while for model His one hydronium (interconverting with water) and one Cl^- counter-ion were used. The derived parameters for the PMF were used to titrate hydroxide and hydronium in water boxes. Small adjustments were done to achieve reference pK_a's of hydroxide and hydronium. The resulting parameters were then tested on titration of model compounds (Asp, Glu, and His).

Simulation protocol

All simulations were carried out using an in-house modified version of CHARMM (version c36b2) (6). The all-atom CpHMD method was implemented in the PHMD module (1) and the pH-based replica-exchange protocol was added to the REPDSTR module (7). The CHARMM22/CMAP additive force field for proteins (8) and the modified CHARMM TIP3P water model (9) were used. It was shown that CHARMM force field underestimates the dielectric constants of alkanes by almost a factor of 2 (10). A smaller dielectric constant for the protein interior results in an overestimation of the desolvation energies of charged sidechains, thereby contributing to a systematic overestimation of the pK_a shifts for buried residues.

The respective partial charges for water, hydroxide and hydronium were taken from TIP3P (9),

CHARMM22 (11), and the work by Sagnella and Voth (12) (see Table S1). The parameters for the bond and angle energy terms for hydronium were from Sagnella and Voth (12). Other force field parameters for hydroxide and hydronium were adapted from TIP3P. To prevent prolonged attraction between hydroxide and hydronium, the van der Waals interaction distance (R_{min}) between oxygen atoms of hydroxide and hydronium was increased to 4.5 Å. The modified R_{min} for sodium, and for sodium-chloride as well as sodium-carbonyl oxygen pairs by Roux and coworkers were used (13, 14). The SHAKE algorithm was applied to all bonds involving hydrogen to allow a 2-fs time step. Non-bonded interactions were truncated at 14 Å, beyond which the electrostatic interactions were treated by the generalized reaction field (GRF) method (1). In the GRF term, $\varepsilon_{\rm in}$ and $\varepsilon_{\rm out}$ were set to 1.0 and 80.0, respectively, and the ionic strength was set to the experimental values as mentioned above. All simulations employed periodic-boundary conditions, and ambient temperature (300 K) and pressure (1 atm) respectively controlled by the Hoover thermostat (15) and Langevin piston pressure-coupling algorithm (16). The titration coordinates were propagated using the Langevin algorithm with a collision frequency of 5 ps^{-1}. The mass of the fictitious λ particles was set to 10 atomic mass units.

For each protein, one set of CpHMD simulations with the pH replica-exchange sampling protocol (7) was performed. The pH range was 1.5–6.5 for HP36, 0.5–8.0 for BBL, and -1.0–9.5 for HEWL. The pH interval was 0.5. Exchanges between adjacent pH replicas were attempted every 500 MD steps or 1 ps. Simulation length was 10 ns per replica.

Supplemental Tables and Figures

Table S1: Atomic partial charges for water, hydroxide and hydronium

Atom	H_2O	OH^-	H_3O^+
OH_2	-0.834	-1.32	-0.755
H1	0.417	0.32	0.585
H2	0.417	0.0	0.585
H3	-	-	0.585

Table S2: Calculated and reference p$K_{\rm a}$ values for model compounds

Model	Calc p$K_{\rm a}$	Calc Hill	Ref p$K_{\rm a}$
Asp	3.5 $\pm$ 0.17	0.99 $\pm$ 0.08	4.0
Glu	4.1 $\pm$ 0.13	0.96 $\pm$ 0.06	4.4
His	6.8 $\pm$ 0.10 (7.3†/7.0‡)	0.97 $\pm$ 0.01	6.45 (6.6†/7.0‡)

The p$K_{\rm a}$ values were calculated based on five independent sets of pH-REX CpHMD simulations, each of which was run with 5 pH replicas and lasted 10 ns per replica. Reference p$K_{\rm a}$'s for Asp and Glu are taken from Nozaki and Tanford (17), while those for His are taken from Bashford (18). †Nδ site. ‡Nϵ site.

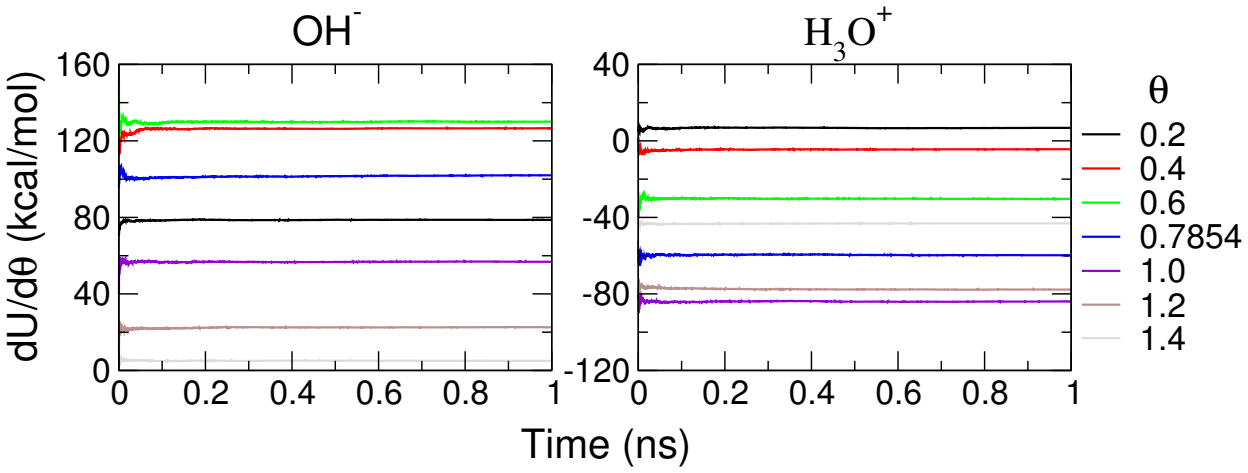

Figure S1: Convergence of the average forces at specified θ values. Calculation was performed cumulatively for hydroxide (*left*) and hydronium (*right*).

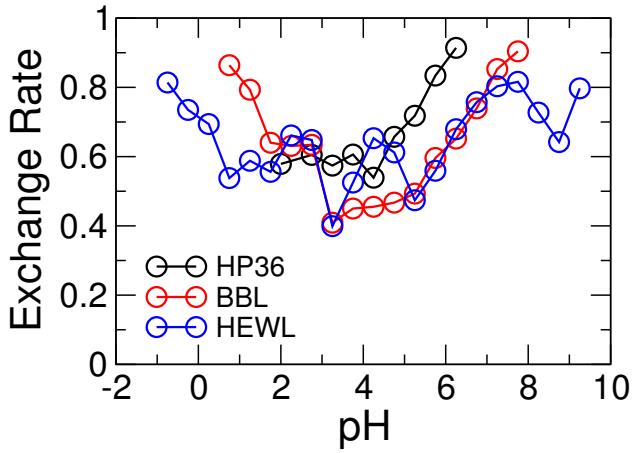

Figure S2: Exchange rates between the adjacent pH replicas in the 10-ns simulations of proteins.

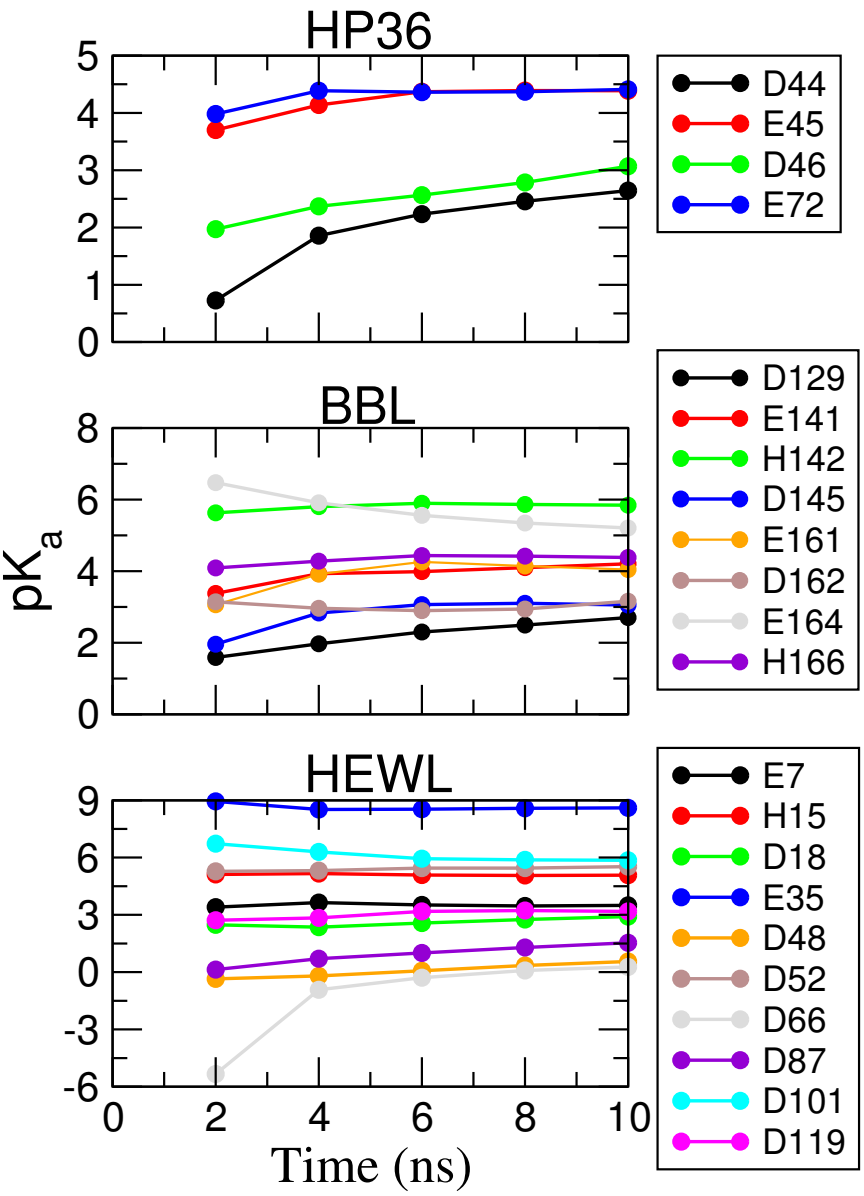

Figure S3: The pK_{a}'s of titratable residues of proteins calculated cumulatively every 2 ns.

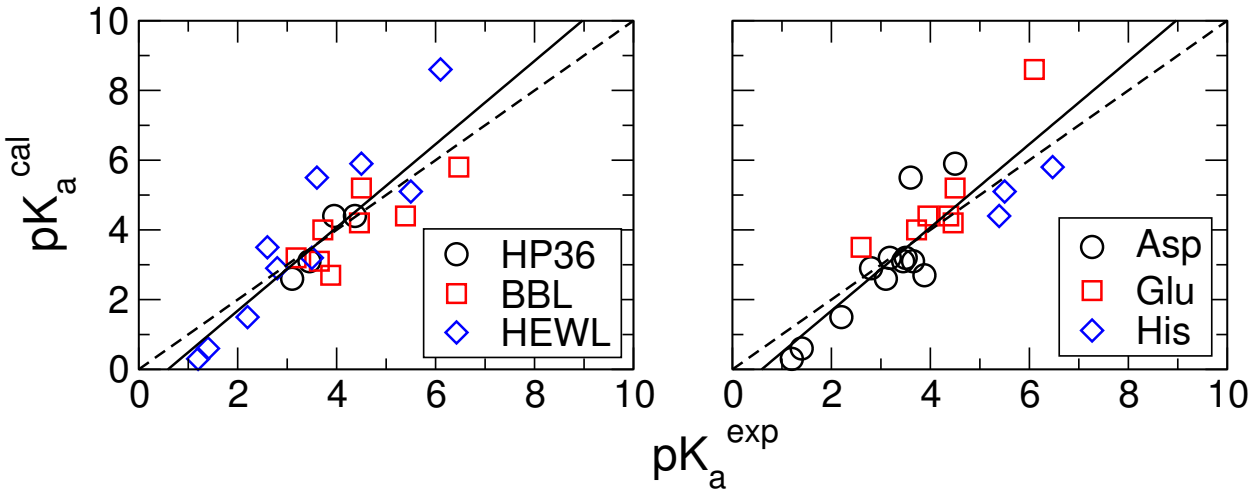

Figure S4: Comparison between calculated and experimental p$K_{\rm a}$'s for different proteins (*left*) and residues (*right*). Calculated p$K_{\rm a}$'s are from the entire 10-ns simulations. The solid line represents the linear regression to the data (slope=1.20 and R^2=0.76).

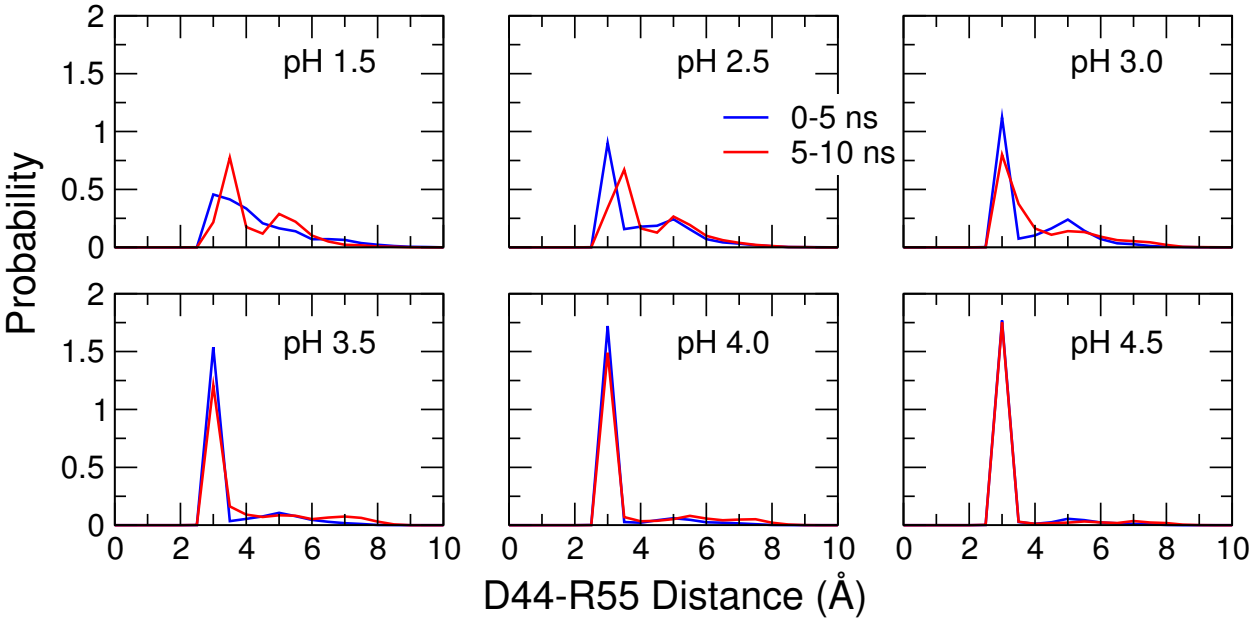

Figure S5: Probability distribution of the minimal distance between the carboxyl oxygen atoms of Asp44 and the guanidino nitrogen atoms of Arg55 in HP36. The first and second 5-ns data are shown in blue and red, respectively.

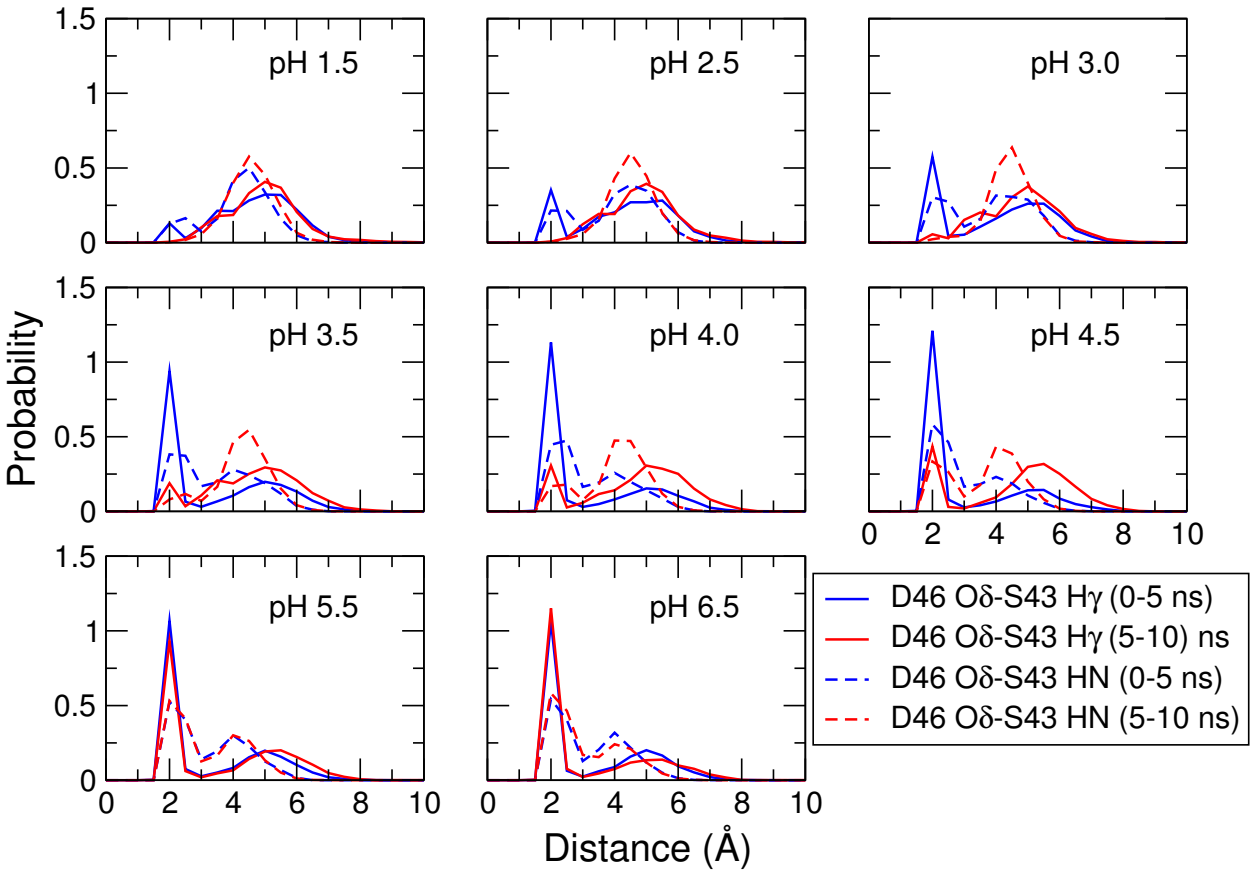

Figure S6: Probability distribution of the minimal distance from the carboxyl oxygen atom of Asp44 to the hydroxyl hydrogen atom (solid lines) and amide hydrogen (dashed lines) of Ser43 in HP36. The first and second 5-ns data are shown in blue and red, respectively.

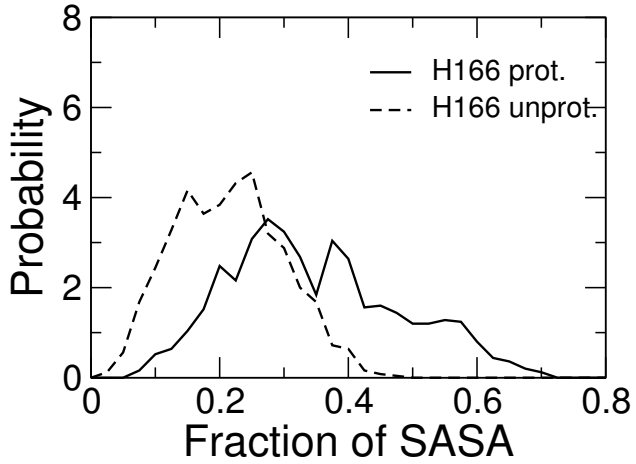

Figure S7: Probability distribution of the fractional SASA for the His166 side chain of BBL when His166 is fully protonated (pH 0.5) and unprotonated (pH 8). The fully solvent-exposed surface area (SASA) for His is 179 $Å^2$.

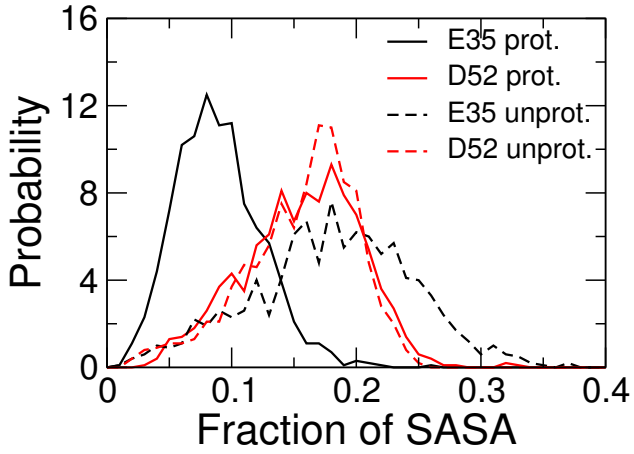

Figure S8: Probability distribution of the fractional SASA of the side chains of Glu35 and Asp52 in HEWL when they are fully protonated (pH 1) and unprotonated (pH 9.5). The fully solvent-exposed surface area (SASA) for Glu is 175 Å^2 and it is 145 Å^2 for Asp.

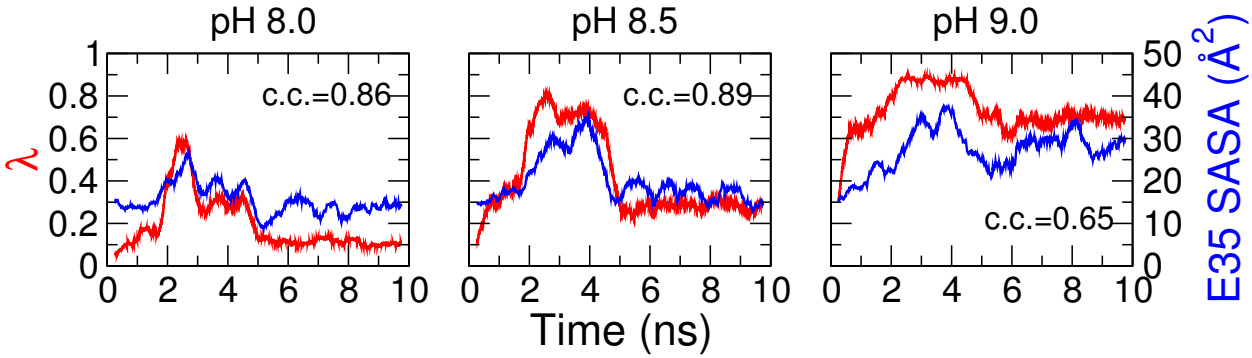

Figure S9: Correlation between the value of titration coordinate λ and the SASA of the side-chain of Glu35 of HEWL. Curves are running averages over 500-ps windows. Correlation coefficients are shown.

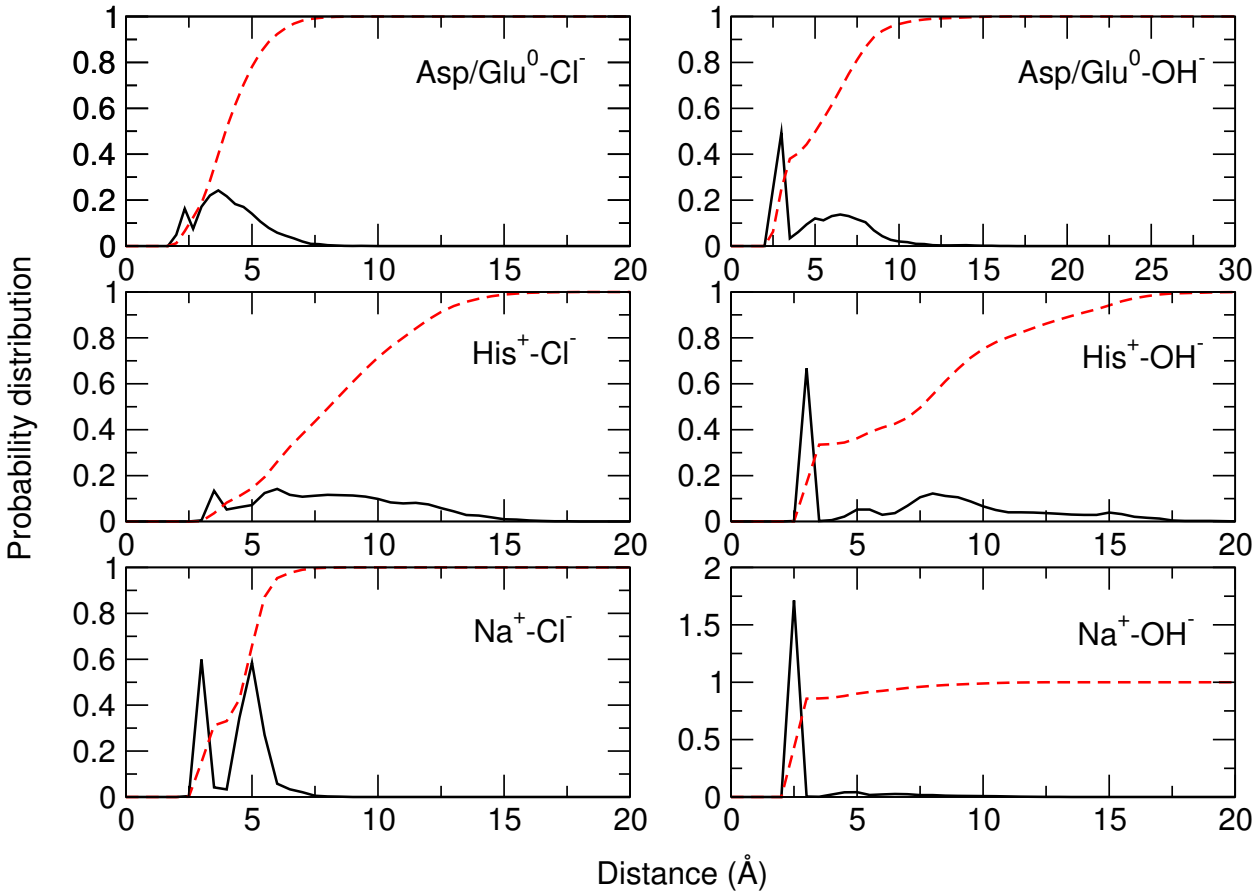

Figure S10: Interactions between the hydroxide and titratable sites/ions in BBL. Interactions in HP36 and HEWL are very similar. Left panel. Probability distribution of the minimum distance from the chloride ions to the carboxylic oxygens of Asp/Glu (top) or sodium ions (bottom). Right panel. Probability distribution of the minimum distance from the hydroxide to the carboxylic oxygens of Asp/Glu (top) or sodium ions (bottom). Dashed red curves are the integrated form (probability). We define the relative occupancy of the hydroxide as the probability when the minimum distance is within 5 Å. While the positions of the peaks are identical for the hydroxide and chloride ions, the major peak is much higher for the former.

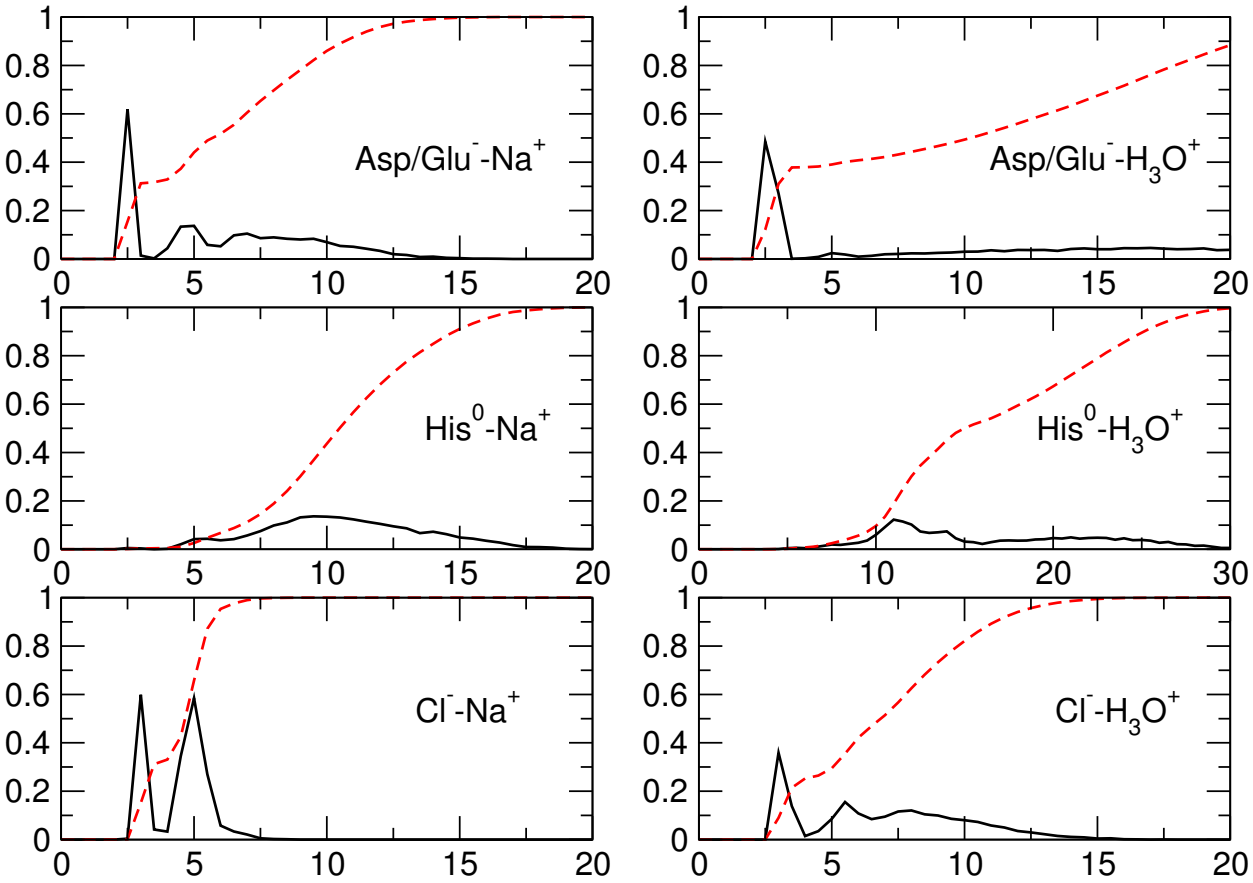

Figure S11: Interactions between the hydronium and titratable sites/ions in BBL. Interactions in HP36 and HEWL are very similar. Left panel. Probability distribution of the minimum distance from the sodium ions to the carboxylic oxygens of Asp/Glu (top) or sodium ions (bottom). Right panel. Probability distribution of the minimum distance from the hydronium to the carboxylic oxygens of Asp/Glu (top) or sodium ions (bottom). Dashed red curves are the integrated form (probability). We define the relative occupancy of the hydroxide as the probability when the minimum distance is within 5 Å.

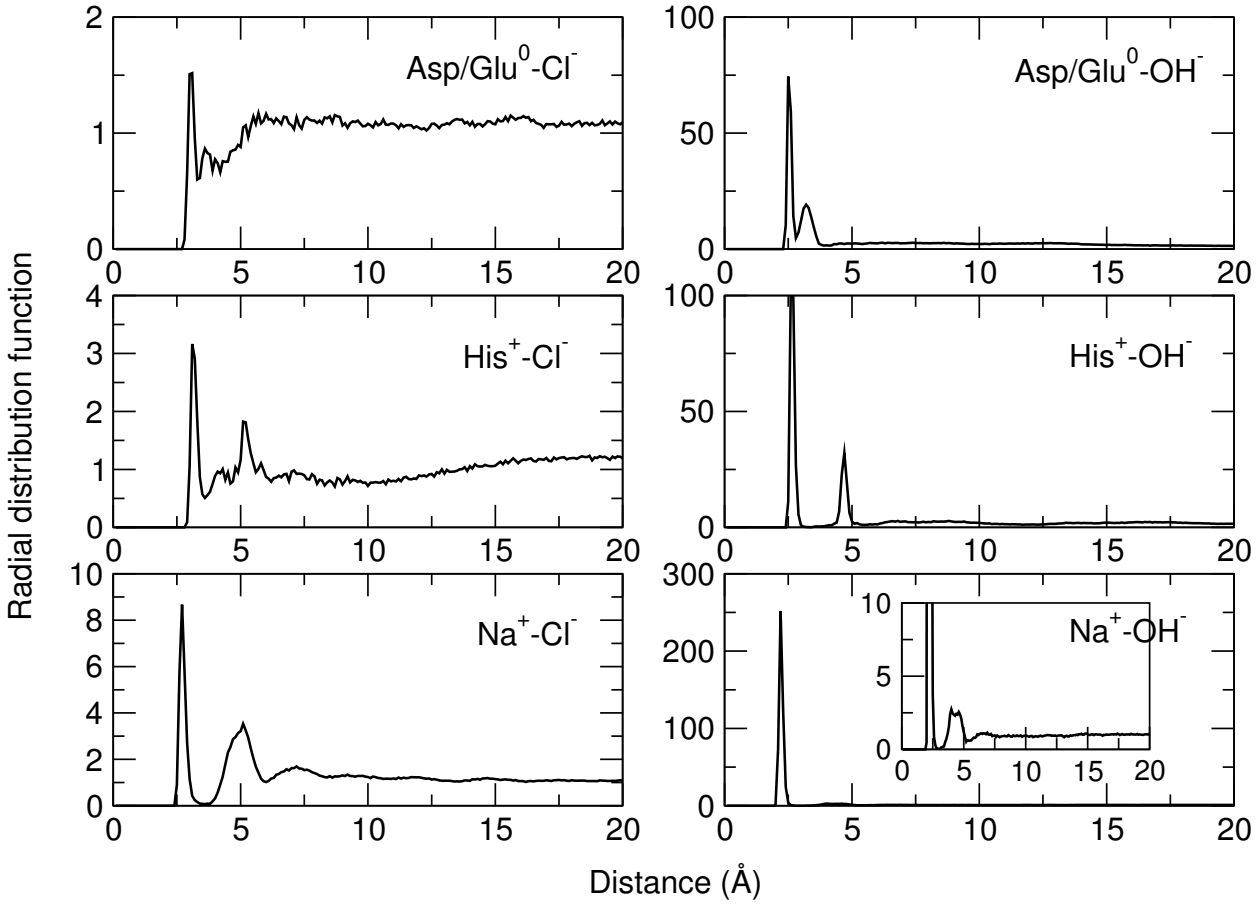

Figure S12: Interactions between hydroxide ions and titratable sites/ions in BBL. Left panel. Radial distribution function (RDF) from the chloride ions to the carboxylic oxygens of Asp/Glu (top) or sodium ions (bottom). Right panel. RDF from the hydroxide to the carboxylic oxygens of Asp/Glu (top) or sodium ions (bottom). RDFs for HP36 and HEWL are very similar. Note a second peak in the sodium-chloride RDF, which is due to the water-bridged interaction. We note that the RDF of Na^+–Cl^- is very similar to that obtained by Luo and Roux using the same force field (14).

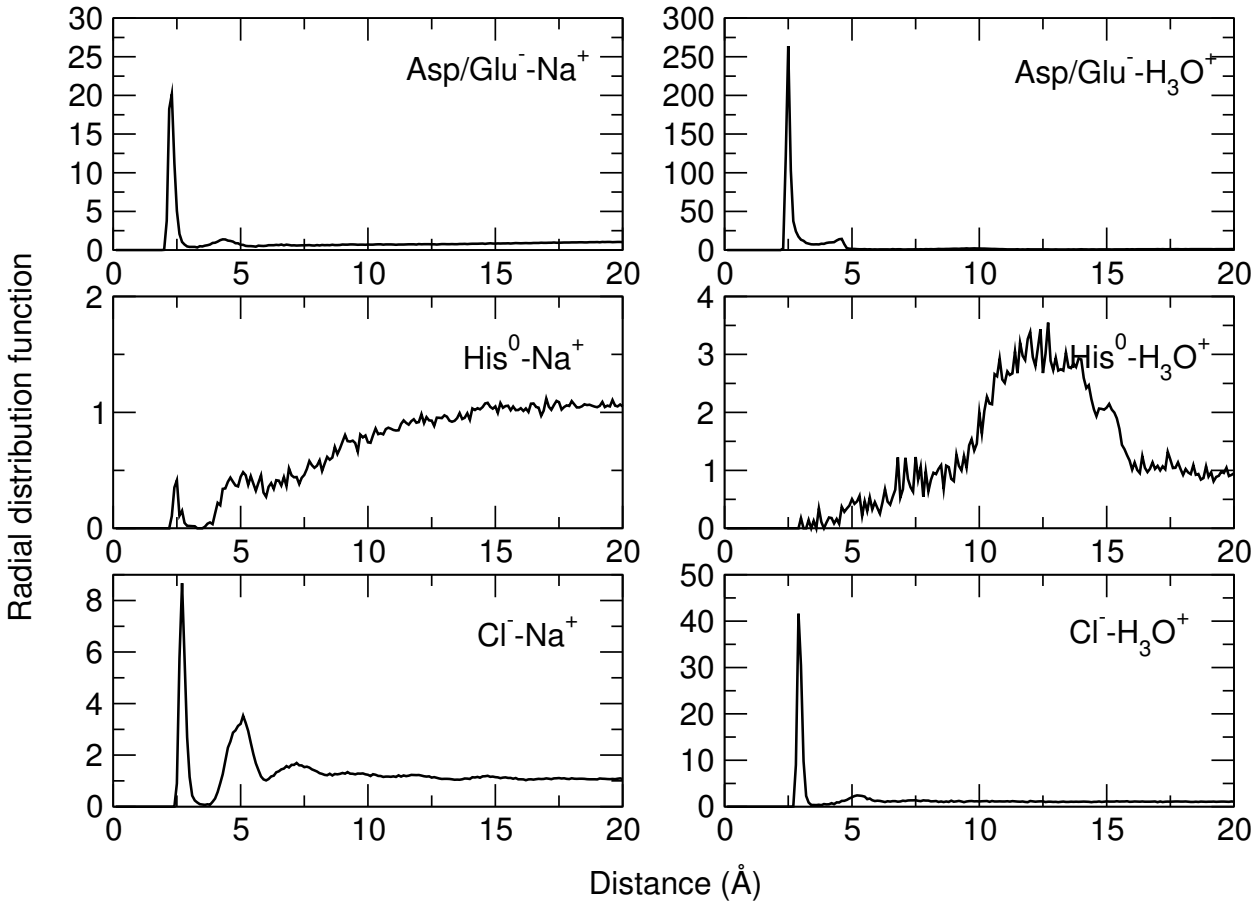

Figure S13: Interactions between hydronium and titratable sites/ions in BBL. Left panel. Radial distribution function (RDF) from chlorides to the carboxylic oxygens of Asp/Glu (top) or sodium ions (bottom). Right panel. RDF from the hydronium to the carboxylic oxygens of Asp/Glu (top) or sodium ions (bottom). RDFs for HP36 and HEWL are very similar. Note a second peak in the sodium-chloride RDF, which is due to the water-bridged interaction. The RDF of acid-Na^+ has two peaks: a major peak at 2.3 Å and a minor peak at 4.3 Å, which is in agreement with the RDF for the formate–Na^+ interaction (19).

References

1. Wallace, J. A., and J. K. Shen, 2012. Charge-leveling and proper treatment of long-range electrostatics in all-atom molecular dynamics at constant pH. *J. Chem. Phys.* 137:184105.

2. Bi, Y., 2008. Studies of the folding and stability of the villin headpiece subdomain. Ph.D. thesis, Stony Brook University.

3. Arbely, E., T. J. Rutherford, T. D. Sharpe, N. Ferguson, and A. R. Fersht, 2009. Downhill versus barrier-limited folding of BBL 1: energetic and structural pertubation effects upon protonation of a histidine of unusually low pKa. *J. Mol. Biol.* 387:986–992.

4. Arbely, E., T. J. Rutherford, H. Neuweiler, T. D. Sharpe, N. Ferguson, and A. R. Fersht, 2010. Carboxyl pK_a values and acid denaturation of BBL. *J. Mol. Biol.* 403:313–327.

5. Webb, H., B. M. Tynan-Connolly, G. M. Lee, D. Farrell, F. O'Meara, C. R. Søndergaard, K. Teilum, C. Hewage, L. P. McIntosh, and J. E. Nielsen, 2011. Remeasuring HEWL pK_a values by NMR spectroscopy: methods, analysis, accuracy, and implications for theoretical pK_a calculations. *Proteins* 79:685–702.

6. Brooks, B. R., C. L. Brooks III, A. D. Mackerell Jr., L. Nilsson, R. J. Petrella, B. Roux, Y. Won, G. Archontis, C. Bartles, S. Boresch, A. Caflisch, L. Caves, Q. Cui, A. R. Dinner, M. Feig, S. Fischer, J. Gao, M. Hodoscek, W. Im, K. K. T. Lazaridis, J. Ma, V. Ovchinnikov, E. Paci, R. W. Pastor, C. B. Post, J. Z. Pu, M. Schaefer, B. Tidor, R. M. Venable, H. L. Woodcock, X. Wu, W. Yang, D. M. York, and M. Karplus, 2009. CHARMM: The biomolecular simulation program. *J. Comput. Chem.* 30:1545–1614.

7. Wallace, J. A., and J. K. Shen, 2011. Continuous constant pH molecular dynamics in explicit solvent with pH-based replica exchange. *J. Chem. Theory Comput.* 7:2617–2629.

8. Mackerell, Jr., A. D., M. Feig, and C. L. Brooks, III, 2004. Extending the treatment of backbone energetics in protein force fields: Limitations of gas-phase quantum mechanics in reproducing protein conformational distributions in molecular dynamics simulations. *J. Comput. Chem.* 25:1400–1415.

9. Jorgensen, W. L., J. Chandrasekhar, J. D. Madura, R. W. Impey, and M. L. Klein, 1983. Comparison of simple potential functions for simulating liquid water. *J. Chem. Phys.* 79:926–935.

10. Vorobyov, I. V., V. M. Anisimov, and A. D. M. Jr., 2005. Polarizable Empirical Force Field for Alkanes Based on the Classical Drude Oscillator Model. *J. Phys. Chem. B* 109:18988–18999.

11. MacKerell Jr., A. D., D. Bashford, M. Bellott, R. L. Dunbrack Jr., J. D. Evanseck, M. J. Field, S. Fischer, J. Gao, H. Guo, S. Ha, D. Joseph-McCarthy, L. Kuchnir, K. Kuczera, F. T. K. Lau, C. Mattos, S. Michnick, T. Ngo, D. T. Nguyen, B. Prodhom, W. E. Reiher III, B. Roux, M. Schlenkrich, J. C. Smith, R. Stote, J. Straub, M. Watanabe, J. Wiórkiewicz-Kuczera, D. Yin, and M. Karplus, 1998. All-atom empirical potential for molecular modeling and dynamics studies of proteins. *J. Phys. Chem. B* 102:3586–3616.

12. Panahi, A., and M. Feig, 1996. Structure and Dynamics of Hydronium in the Ion Channel Gramicidin A. *Biophys. J.* 70:2043–2051.

13. Noskov, S. Y., and B. Roux, 2008. Control of ion selectivity in LeuT: two Na^+ binding sites with two different mechanisms. *J. Mol. Biol.* 377:804–818.

14. Luo, Y., and B. Roux, 2010. Simulation of osmotic pressure in concentrated aqueous salt solutions. *J. Phys. Chem. Lett.* 1:183–189.

15. Hoover, W. G., 1985. Canonical dynamics: Equilibration phase-space distributions. *Phys. Rev. A* 31:1695–1697.

16. Feller, S. E., Y. Zhang, R. W. Pastor, and B. R. Brooks, 1995. Constant pressure molecular dynamics simulation: The Langevin piston method. *J. Chem. Phys.* 103:4613–4621.

17. Nozaki, Y., and C. Tanford, 1967. Examination of titration behavior. *Methods Enzymol.* 11:715–734.

18. Bashford, D., D. A. Case, C. Dalvit, L. Tennant, and P. E. Wright, 1993. Electrostatic calculations of side-chain pK_a a values in myoglobin and comparison with NMR Data for histidines? *Biochemistry* 32:8045–8056.

19. Jagoda-Cwiklik, B., R. Vacha, M. Lund, M. Srebro, and P. Jungwirth, 2007. Ion pairing as a possible clue for discriminating between sodium and potassium in biological and other complex environments. *J. Phys. Chem. B* 111:14077–14079.